Supplementary Methods

Mouse lung cancer allograft assay and treatments

A total of 1×10^6 KP, KL or LLC cells were injected subcutaneously into the bilateral flanks of female C57BL/6 mice, respectively. The treatment was administered when the tumor volume (calculated as width × length) reached approximately 50 mm^2. All cryoablation procedures were carried out only on the left tumor, using the Cryotherapy System device and a 1.2-mm-diameter cryoprobe (AccuTarget MediPharma [Shanghai] Co., Ltd.), which used nitrogen as the refrigerant. The tip of the cryoprobe was inserted into the tumor along its long axis, and then 2 freeze-thaw cycles (20 and 10 seconds, respectively, for each cycle) were performed. During the freezing phase, the temperature at the tip of the cryoprobe could reached below -80℃. The target tumor was entirely covered by the ice ball to ensure complete ablation. The growth of contralateral tumors was monitored every 2 days.

IFNAR1 blockade was accomplished by administering 400 μg anti-IFNAR1 (clone MAR1-5A3, BioXCell) or isotype control monoclonal antibody (BioXCell) intraperitoneally every 3 days for a total of 4 doses. For PD-1 blockade, 200 μg anti–PD-1 (clone MP1-14, BioXCell) or isotype control monoclonal antibody (BioXCell) was administered intraperitoneally at day 1, 4, 7 and 10 after cryoablation (figure 6B).

Sham treatment and cryoablation

The treatment was administered when the tumor volume (calculated as width × length) reached approximately 50 mm^2. The experimental grouping is shown in supplementary figure S2A. In non-CA group, no treatment was received. In sham treatment group, cryoprobe was inserted into

the left tumor without cryoablation. In sham CA group, CA was performed in subcutaneous tissue ensuring no damage to the implanted tumor. In CA group, CA was performed in tumor tissues. The growth of contralateral tumors was monitored every 2 days.

Data analysis for bulk RNA sequencing

Genome index and raw gene expression matrix for each sample were generated from raw fastq data using *STAR* (v2.7.6a) [1]. The combined gene expression matrix was then generated by customized scripts for *R* (v4.1.3). Subsequently, the gene expression matrix was converted to a DESeqDataSet object using *DESeq2* R package (v1.34.0) [2]. Normalization was performed by *DESeq2* and DEGs were selected by adjusted p-value < 0.05. Gene set signatures were computed using the average gene expression and *GSVA* (v1.42.0) R package based on Hallmark gene sets (h.all.v7.4.symbols.gmt) and some manually curated pathways. To visualize gene expression and gene set activity, the heatmaps were generated using *ComplexHeatmap* R package (v2.10.0) [3].

Flow cytometric analysis

Preparation of mouse tumors

Freshly harvested tumors were treated with the Mouse Tumor Dissociation Kit (Miltenyi Biotec) to generate single-cell suspension for flow cytometry following the manufacturer's instructions. Subsequently, the dissociated tumor samples were filtered through a 70-μm strainer, followed by centrifugation using Percoll reagent (GE) to enrich immune cells. Erythrocytes were lysed with lysis buffer (Beyotime) for 5 min at RT and washed twice with PBS.

Staining

To detect intracellular cytokine production, cells were stimulated with Cell Stimulation Cocktail (plus protein transport inhibitors) (1:500, eBioscience) for 4 hours in a 37°C and 5% CO_2 incubator, and washed twice with FACS buffer (PBS + 2% FBS + 1mM EDTA) before staining. For live-dead discrimination, cells were stained with Zombie UV™ Fixable Viability Kit (Biolegend) for 30 min at RT in the dark. For surface marker analysis, cells were stained with indicated fluorochrome-conjugated antibodies in FACS buffer for 30 minutes. For intracellular marker staining, the Transcription Factor Buffer Set (BD Pharmingen) was utilized following the manufacturer's instructions, and then stained with indicated fluorochrome-conjugated antibodies. All samples were washed with washing buffer (BD Pharmingen) after each staining. At last, all samples further passed through a 70-μm cell strainer. The antibodies used for flow cytometry staining were listed in supplemental table S2. Flow cytometry was performed using BD FACS Fortessa. Data were analyzed with FlowJo 10.8.1 software. Appropriate isotype controls were used as negative controls.

Quality control, determination of major cell lineages and subclustering of T cells and myeloid populations

CellRanger (v6.0.1) *count* was used to aggregate the raw gene expression matrix from the initial raw fastq data of each sample, which was converted to a Seurat object using *Seurat* R package (v4.1.1) [4]. The gene expression was normalized by the SCT method [5] and a total of 17,670 and 40,917 high-quality cells were finally obtained for $CD45^+$ and $CD45^+CD3^+$ scRNA-seq respectively. Cell clusters projected in the two-dimensional *UMAP* representation were annotated to known cell types using well-recognized marker genes.

To further identify subpopulations within the major cell clusters from $CD45^+$ 3' scRNA-seq, a second-round data process, dimension reduction and cell type annotation were performed for T and myeloid cells separately. The subset gene expression matrix was normalized by the *LogNormalize* method, and a total of 12 subclusters were obtained. To validate the accuracy of our annotation results, *ProjecTIL* analysis [6] (*ProjecTILs* R package, v2.0.0) was performed with the 'mouse TIL atlas' as a reference atlas, and most of cell types were well-matched. Myeloid cells, including mast cells, underwent a similar re-clustering pipeline as T cells, resulting in the identification of 8 clusters.

Analysis of pathway enrichment and gene signatures

DEGs were identified using the Wilcoxon Rank Sum test between the non-CA and CA groups, either across all cells or within specific cell clusters by *Seurat* R package with default parameters. A maximum of 120 DEGs with a logFC_threshold > 0.25 were selected. GO enrichment analysis was performed with *clusterProfiler* R package (v4.2.2) based on the up-regulated DEGs in the CA group. The results were visualized through barplots generated by *ggplot2* R package (v3.4.1).

Gene set signatures from both bulk RNA-seq and 3' scRNA-seq, including the effector signature, cytolytic score and IFN response signature of $CD8^+$ T cells, and type I IFN production were computed using the average gene expression and *GSVA* (v1.42.0) R package based on Hallmark gene sets (h.all.v7.4.symbols.gmt), GO gene sets (c5.go.v7.4.symbols.gmt) from MSigDB and some manually curated pathways. Naïve and exhaustion scores of $CD8^+$ T cells were performed by a customized R script, following the methodology established by Gong et al [7]. In brief, logistic regression models were developed for each gene module and corresponding cell

clusters, and then the module score for each cell was calculated by summing the product of each gene expression and weights estimated from the model parameters. The heatmap was plotted using *ComplexHeatmap* with P-value and Z-score computed by R, and the boxplots were plotted using *ggplot2* with statistical tests performed by *ggpubr* R package (v0.4.0).

Pseudotime trajectory analysis of CD8$^+$ T cells and myeloid populations

Pseudotime trajectory analysis of CD8$^+$ T cells was performed by *Monocle v3* R package (v1.0.0) [8]. Pseudotime values were calculated, and the trajectory paths and directions were computed. *Monocle v3* and *ggplot2* R package were used to visualize the pseudotime trajectory. Pseudotime trajectory analysis of Myeloid cells was performed by *Monocle v2* R package (v2.22.0) [9]. The two-dimensional components and pseudotime values by *Monocle v2* were merged into the Seurat object, and *Seurat* and *ggplot2* were used to visualize the pseudotime trajectory.

Clonotype diversity analysis and CoNGA

Immunarch R package (v0.8.0) was applied to read and process the clonotype data from outputs of *CellRanger vdj*. The clonotype data was then integrated with cell attributes from scRNA-seq data based on shared cell barcodes. The clonal expansion score, as defined by Wang et al. [10], was calculated and compared in T cell clusters between non-CA and CA groups.

To enhance the integration of information between scRNA-seq and scTCR-seq, we performed *CoNGA* (*CoNGA* python package, v0.1) analysis [11]. In brief, CoNGA uses TCRdist to cluster immune repertoire (IR) data and generate a cell-cell relationship network from the IR. Simultaneously, it generates a cell-cell relationship network from gene expression (GEX) using

Scanpy. Subsequently, CoNGA integrates the GEX and IR networks by identifying nodes that share similar neighbors in both networks. By employing CoNGA approach, we acquired 23,739 paired cells which was reduced into 15,055 clones. Each clone was assigned a CoNGA score through the *CoNGA* pipeline.

Multiplex immunoassay

The mouse tumor tissues were homogenized (1:9) in PBS for 4 minutes, and then were centrifuged at 12,000 rpm for 5 minutes at 4°C. Supernatants were collected and the protein level of IFN-α and IFN-β was detected using LEGENDplex™ Mouse Type 1/2 Interferon Panel (Biolegend) according to the manufacturer's instructions. Briefly, 25μl supernatant or standard was mixed with 25μl assay buffer and mixed capture beads, and then incubated for 2 hours at room temperature. After washing the plate, 25μl detection antibodies were added to each well and incubated for 1 hour at room temperature. Then SA-PE was added directly and incubated for 30 min at room temperature. After washing, all samples were read on Beckman Coulter CytoFLEX S. The assay FCS files were analyzed to calculate the concentration of IFN-α and IFN-β using BioLegend's LEGENDplex™ data analysis software.

Western blot analysis

Mouse tumor tissues were lysed using RIPA lysis buffer (P0013B, Beyotime) containing a protease inhibitor (1:100, Beyotime) and a phosphatase inhibitor (1:100, Epizyme). Approximately 30–50 μg of total protein was separated on 10% SDS-PAGE, transferred onto a 0.45-μm PVDF membrane, blocked with 5% non-fat milk, and incubated overnight at 4 °C with

primary antibodies against indicated antibodies (supplementary table S2). Antibodies were removed from the membrane by incubation with stripping buffer (Beyotime) for 15 min.

Statistics

All statistical analyses in the experiments were performed using SPSS 25.0 (IBM, New York, NY, USA) and GraphPad Prism 8.0 (GraphPad Software, San Diego, California, USA). *P*-value ≤ 0.05 was considered significant difference. Data are expressed as mean ± SEM. The two-sided unpaired Student's t-test was used for comparison of two groups (non-CA and CA group; before and after the cryoablation). ANOVA test was used for comparisons of groups in studies involving combined therapy (PD-1 blockade and IFNAR-1 blockade). Survival curves were analyzed by log-rank (Mantel Cox) test.

All statistical analyses of omics data were performed using R (v4.1.3). Z-score normalization was applied for better visualization in the heatmap. *P*-value ≤ 0.05 was considered significant difference. The one-sided unpaired Student's t-test was used for comparison of gene expression and signature scores between the non-CA and CA groups in bulk RNA-seq data. For single-cell analysis, comparisons between two groups were performed using the nonparametric Wilcoxon rank sum test with Bonferroni correction.

References

1. Dobin A, Davis CA, Schlesinger F et al. STAR: ultrafast universal RNA-seq aligner. Bioinformatics 2013; 29: 15-21.
2. Anders S, Huber W. Differential expression analysis for sequence count data. Genome Biol

2010; 11: R106.

3. Gu Z, Eils R, Schlesner M. Complex heatmaps reveal patterns and correlations in multidimensional genomic data. Bioinformatics (Oxford, England) 2016; 32: 2847-2849.

4. Hao Y, Hao S, Andersen-Nissen E, Mauck WM, 3rd, Zheng S, Butler A, et al. Integrated analysis of multimodal single-cell data. Cell. 2021;184(13):3573-87 e29.

5. Hafemeister C, and Satija R. Normalization and variance stabilization of single-cell RNA-seq data using regularized negative binomial regression. *Genome Biol.* 2019;20(1):296.

6. Andreatta M, Corria-Osorio J, Muller S, Cubas R, Coukos G, and Carmona SJ. Interpretation of T cell states from single-cell transcriptomics data using reference atlases. *Nat Commun.* 2021;12(1):2965.

7. Gong L, Kwong DL, Dai W, Wu P, Li S, Yan Q, et al. Comprehensive single-cell sequencing reveals the stromal dynamics and tumor-specific characteristics in the microenvironment of nasopharyngeal carcinoma. *Nat Commun.* 2021;12(1):1540.

8. Cao J, Spielmann M, Qiu X, Huang X, Ibrahim DM, Hill AJ, et al. The single-cell transcriptional landscape of mammalian organogenesis. *Nature.* 2019;566(7745):496-502.

9. Qiu X, Mao Q, Tang Y, Wang L, Chawla R, Pliner HA, et al. Reversed graph embedding resolves complex single-cell trajectories. *Nat Methods.* 2017;14(10):979-82.

10. Wang J, Xu Y, Chen Z, Liang J, Lin Z, Liang H, et al. Liver Immune Profiling Reveals Pathogenesis and Therapeutics for Biliary Atresia. *Cell.* 2020;183(7):1867-83 e26.

11. Schattgen SA, Guion K, Crawford JC, Souquette A, Barrio AM, Stubbington MJT, et al. Integrating T cell receptor sequences and transcriptional profiles by clonotype neighbor graph analysis (CoNGA). *Nat Biotechnol.* 2022;40(1):54-63.

177

Supplemental Table S1. Mouse primers used in this study

Gene	Forward Primer (5'-3')	Reverse Primer (5'-3')
Il21	GGACCCTTGTCTGTCTGGTAG	TGTGGAGCTGATAGAAGTTCAGG
Ccl5	GCTGCTTTGCCTACCTCTCC	TCGAGTGACAAACACGACTGC
Ccl17	TACCATGAGGTCACTTCAGATGC	GCACTCTCGGCCTACATTGG
Ccl22	AGGTCCCTATGGTGCCAATGT	CGGCAGGATTTTGAGGTCCA
Cxcl9	GGAGTTCGAGGAACCCTAGTG	GGGATTTGTAGTGGATCGTGC
Tnf	CCCTCACACTCAGATCATCTTCT	GCTACGACGTGGGCTACAG
Ifna	TGACCTCAAAGCCTGTGTGATG	AAGTATTTCCTCACAGCCAGCAG
Ifnb	AGCTCCAAGAAAGGACGAACAT	GCCCTGTAGGTGAGGTTGATCT
Cd274	GCTCCAAAGGACTTGTACGTG	TGATCTGAAGGGCAGCATTTC
β-actin	TGTCCACCTTCCAGCAGATGT	AGCTCAGTAACAGTCCGCCTAG

178

Supplemental Table S2. The antibodies used for flow cytometry, WB and multiple-color fluorescence IHC

Antibodies	Clone	Source	Identifier
Zombie UV™ Fixable Viability Kit	/	Biolegend	Cat# 423107
BV510 anti-mouse CD45	30-F11	Biolegend	Cat# 103138
AF700 anti-mouse CD3	17A2	Biolegend	Cat# 100216
FITC anti-mouse CD4	RM4-5	Biolegend	Cat# 100510
PerCP/Cyanine5.5 anti-mouse CD8a	53-6.7	Biolegend	Cat# 100734
BV605 anti-mouse NK1.1	PK136	Biolegend	Cat# 108753
BV605 anti-mouse PD-1	29F.1A12	Biolegend	Cat# 135220
BV421 anti-mouse CD25	PC61	Biolegend	Cat# 102043
PE anti-mouse FOXP3	NRRF-30	eBioscience	Cat# 12-4771-82
PE/Dazzle 594 anti-mouse IFN-γ	XMG1.2	Biolegend	Cat# 505846
PE anti-mouse TNF-α	MP6-XT22	Biolegend	Cat# 506306
PE/Cyanine7 anti-human/mouse Granzyme B	QA16A02	Biolegend	Cat# 372214
BV510 anti-human CD45	HI30	Biolegend	Cat# 304036
PerCP/Cyanine5.5 anti-human CD3	OKT3	Biolegend	Cat# 317226
AF700 anti-human CD4	OKT4	Biolegend	Cat# 317426
APC/Cyanine7 anti-human CD8	SK1	Biolegend	Cat# 344714
BV605 anti-human CD45RA	HI100	Biolegend	Cat# 304134
BV421 anti-human CD197 (CCR7)	G043H7	Biolegend	Cat# 353208
PE/Dazzl 594 anti-human FOXP3	206D	Biolegend	Cat# 320126
Rabbit anti-mouse p-STING (Ser365) mAb	D8W4F	CST	Cat# 72971
Rabbit anti-mouse STING mAb	D2P2F	CST	Cat# 13647
Rabbit anti-mouse p-TBK1/NAK (Ser172) mAb	D52C2	CST	Cat# 5483
Rabbit anti-mouse TBK1/NAK mAb	D1B4	CST	Cat# 3504
Rabbit anti-mouse β-Actin mAb	13E5	CST	Cat# 4970
Anti-rabbit IgG, HRP-linked Antibody	7074S	CST	Cat# 7074
Mouse monoclonal anti-human Pan-CK	AE1/AE3	Abcam	Cat# ab27988
Rabbit monoclonal anti-human CD4	EPR6855	Abcam	Cat# ab133616
Mouse monoclonal anti-human CD8 alpha	C8/144B	Abcam	Cat# ab17147

179

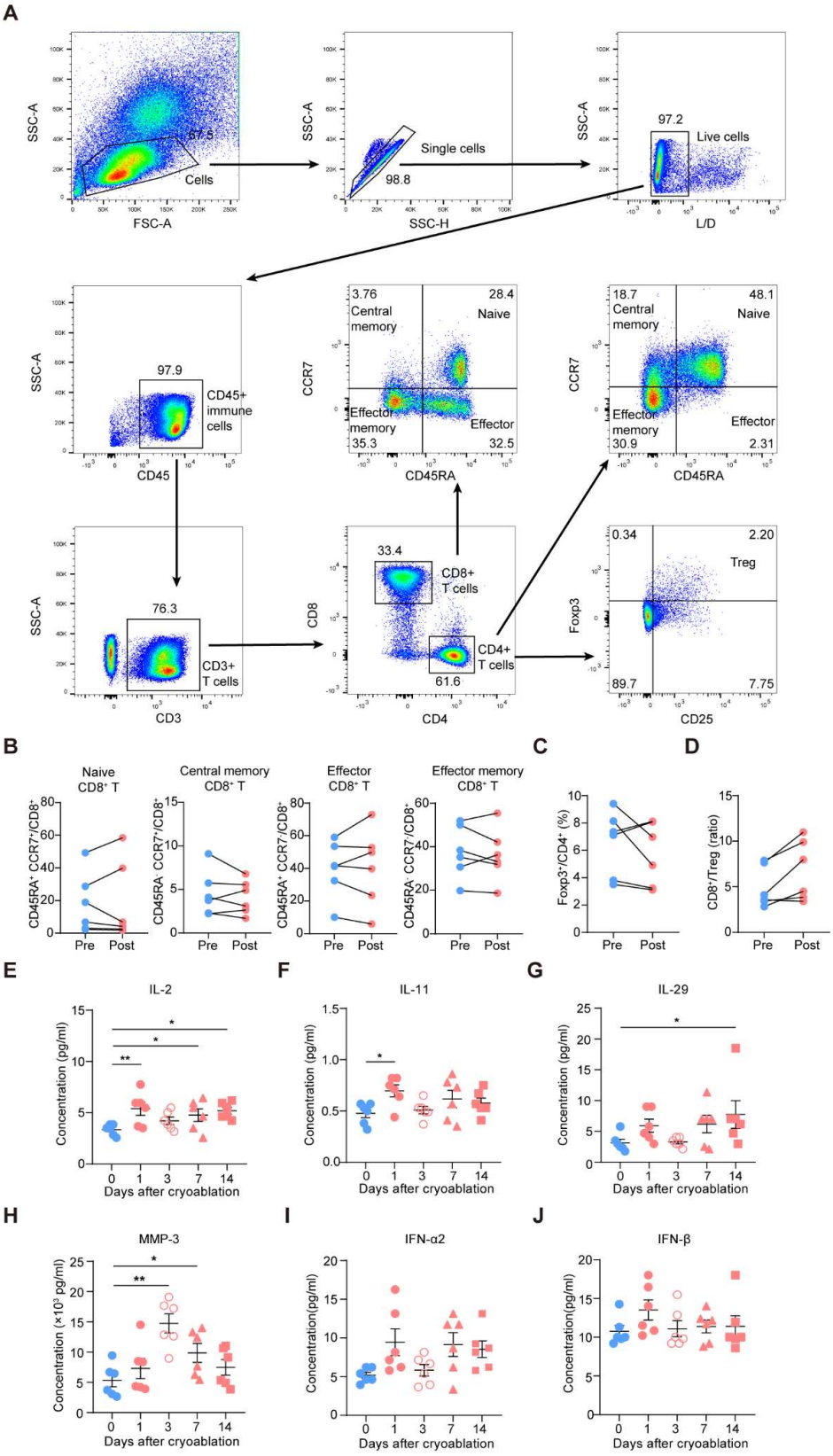
A
SSC-A
FSC-A
67.5
Cells
Single cells
98.8
SSC-H
97.2
Live cells
L/D
97.9
CD45+ immune cells
CD45
3.76
Central memory
28.4
Naive
Effector memory
35.3
Effector
32.5
CCR7
CD45RA
18.7
Central memory
48.1
Naive
Effector memory
30.9
Effector
2.31
76.3
CD3+ T cells
CD3
33.4
CD8+ T cells
CD8
CD4+ T cells
61.6
CD4
0.34
2.20
Treg
89.7
7.75
Foxp3
CD25
B
Naive CD8+ T
Central memory CD8+ T
Effector CD8+ T
Effector memory CD8+ T
CD45RA+ CCR7+/CD8+
CD45RA- CCR7+/CD8+
CD45RA+ CCR7-/CD8+
CD45RA- CCR7-/CD8+
Pre
Post
C
Foxp3+/CD4+ (%)
D
CD8+/Treg (ratio)
E
IL-2
F
IL-11
G
IL-29
Concentration (pg/ml)
Days after cryoablation
H
MMP-3
Concentration (×10³ pg/ml)
I
IFN-α2
J
IFN-β
Concentration(pg/ml)

180

Supplementary Figure S1. The effect of cryoablation on peripheral blood from early-stage NSCLC patients.

(A) The gating strategy of flow cytometric analysis on peripheral blood mononuclear cells.

(B-D) The changes in the percentage of subpopulations of CD8+ T cells (B), the percentage of Foxp3+ Tregs (C) and the ratio of CD8+ T cells to Tregs (D) in the peripheral blood samples collected before cryoablation and at day 1 after cryoablation from early-stage NSCLC patients (n = 6).

(E-J) The changes in the levels of IL-2, IL-11, IL-29, MMP-3, IFN-α and IFN-β secretion in the peripheral blood samples collected before cryoablation and at day 1, 3, 7 and 14 after cryoablation from early-stage NSCLC patients (n = 6).

The results are shown as the mean ± SEM. The statistical significance of differences between two groups was determined by unpaired Student's t-test and the statistical significance of differences among multiple groups was determined by one-way ANOVA. *, $P < 0.05$; **, $P < 0.01$. IL, interleukin; IFN, interferon; MMP, matrix metalloproteinase; NSCLC, non-small cell lung cancer; SSC, side scatter.

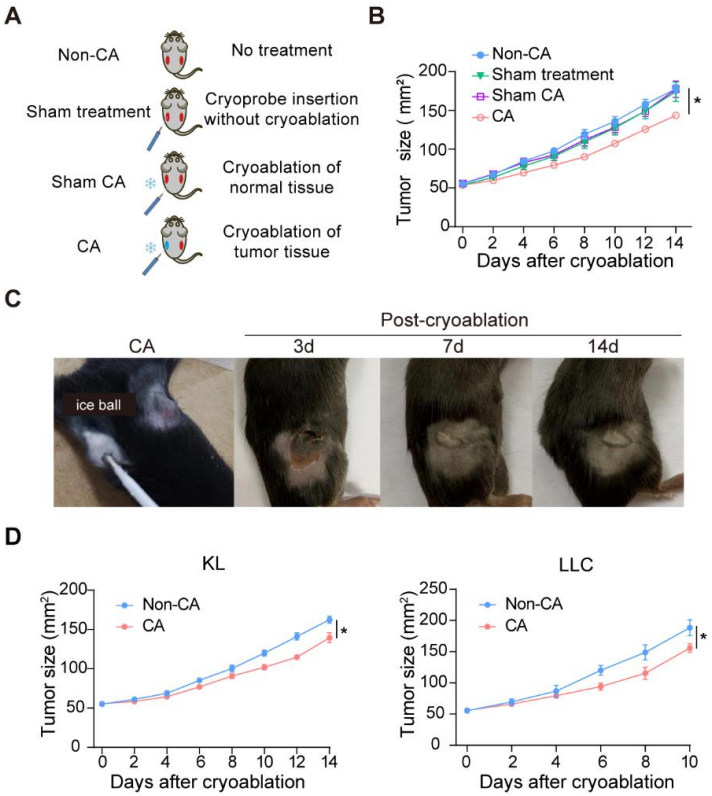

Supplementary Figure S2. The effect of cryoablation on tumor growth.

(A) The experimental design. In non-CA group, no treatment was received. In sham treatment group, the cryoprobe was inserted into the left tumor without cryoablation. In sham CA group, CA was performed in subcutaneous tissue and skin ensuring no damage to the implanted tumor. In CA group, CA was performed in tumor tissues.

(B) Mean tumor growth of the contralateral KP tumors in the non-CA, sham treatment, sham CA and CA groups (n=5 per group).

(C) The changes of the cryoablated tumor during cryoablation and at day 3, 7 and 14 after cryoablation.

(D) Mean tumor growth of the contralateral KL and Lewis lung cancer (LLC) tumors in the non-CA and CA groups (n = 6 per group).

The results are shown as the mean ± SEM. The statistical significance of differences between two groups was determined by unpaired Student's t-test. *, $P < 0.05$. CA, cryoablation; non-CA, non-cryoablation.

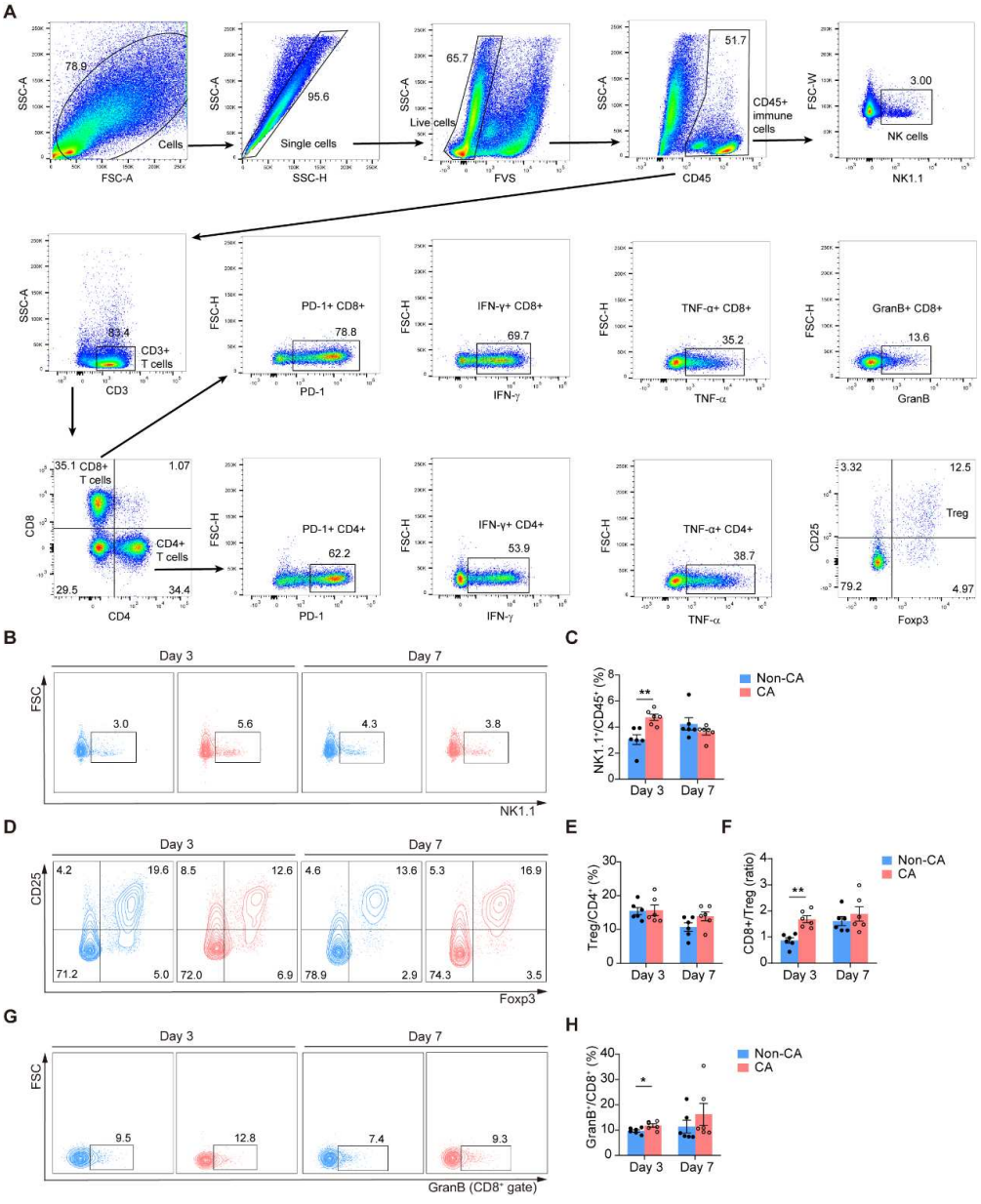

Supplementary Figure S3. Regulation of immune cell infiltration in contralateral KP tumors by cryoablation.

(A) The gating strategy of flow cytometric analysis on KP tumor infiltrating immune cells.

(B and C) Representative flow cytometric plots (B) and the percentage (C) of NK1.1+ natural killer (NK) cells in contralateral KP tumors from the non-CA and CA groups at day 3 and 7 after

cryoablation (n = 6 per group).

(D and E) Representative flow cytometric plots (D) and the percentage (E) of CD25+Foxp3+ Tregs in contralateral KP tumors from the non-CA and CA groups at day 3 and 7 after cryoablation (n = 6 per group).

(F) The ratio of CD8+ TILs to Tregs in the non-CA and CA groups (n = 6 per group).

(G and H) Representative flow cytometric plots (G) and the percentage (H) of GranB+CD8+ TILs in contralateral KP tumors from the non-CA and CA groups at day 3 and 7 after cryoablation (n = 6 per group).

The results are shown as the mean ± SEM, and the statistical significance of differences between groups was determined by an unpaired Student's t-test. *, $P < 0.05$; **, $P < 0.01$. CA, cryoablation; non-CA, non-cryoablation.

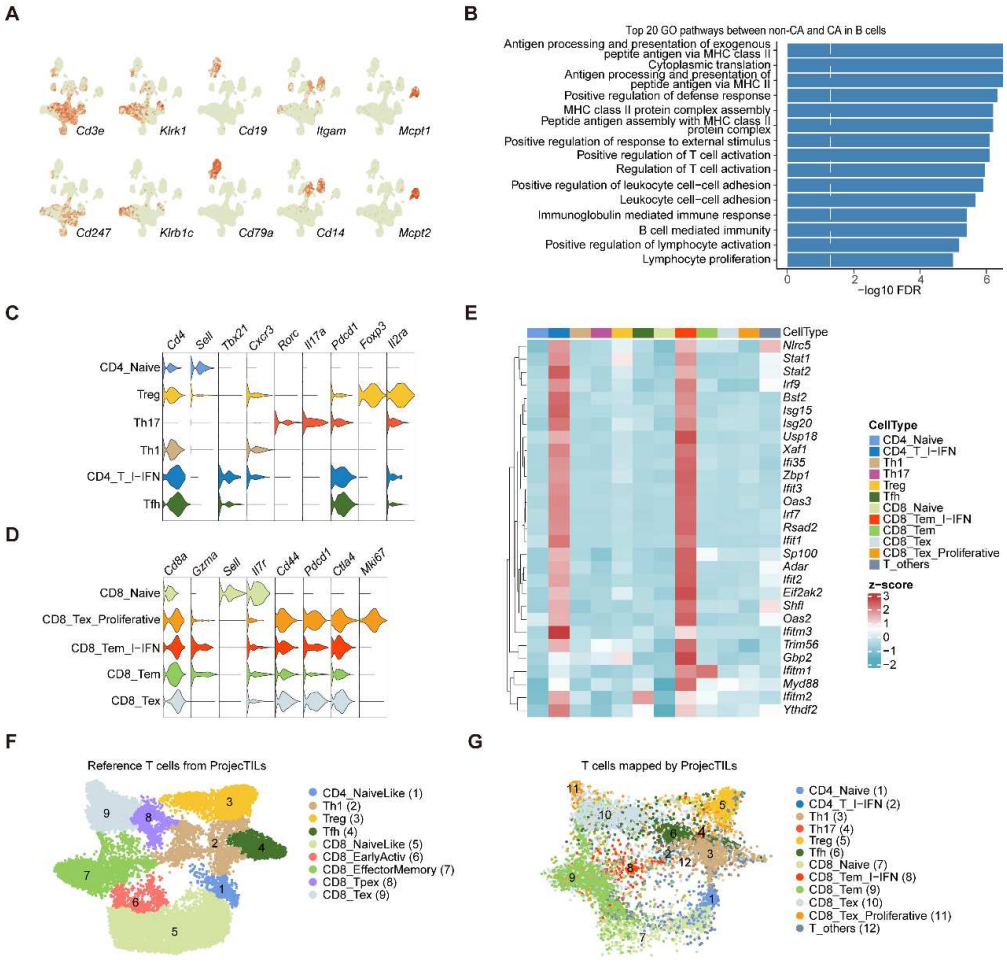

Supplementary Figure S4. Transcriptional profiling of tumor-infiltrating immune cells.

(A) Single-cell transcription level of representative genes illustrated in the UMAP plot of tumor-infiltrating CD45+ immune cells.

(B) GO pathway enrichment analysis of B cells based on the DEGs between the non-CA and CA groups.

(C and D) Single-cell transcription level of representative genes from CD4+ (C) and CD8+ (D) TILs illustrated in the UMAP plot of CD3+CD45+ T cells.

(E) Heatmap showing expression of type I IFN-related genes in each T cell type.

(F and G) Validation of T cells clustering using ProjecTIL. The graphs represent a reference altas

241 from ProjecTILs (F)and our clustering of T cells mapped by ProjecTILs (G).

242 CA, cryoablation; non-CA, non-cryoablation.

243

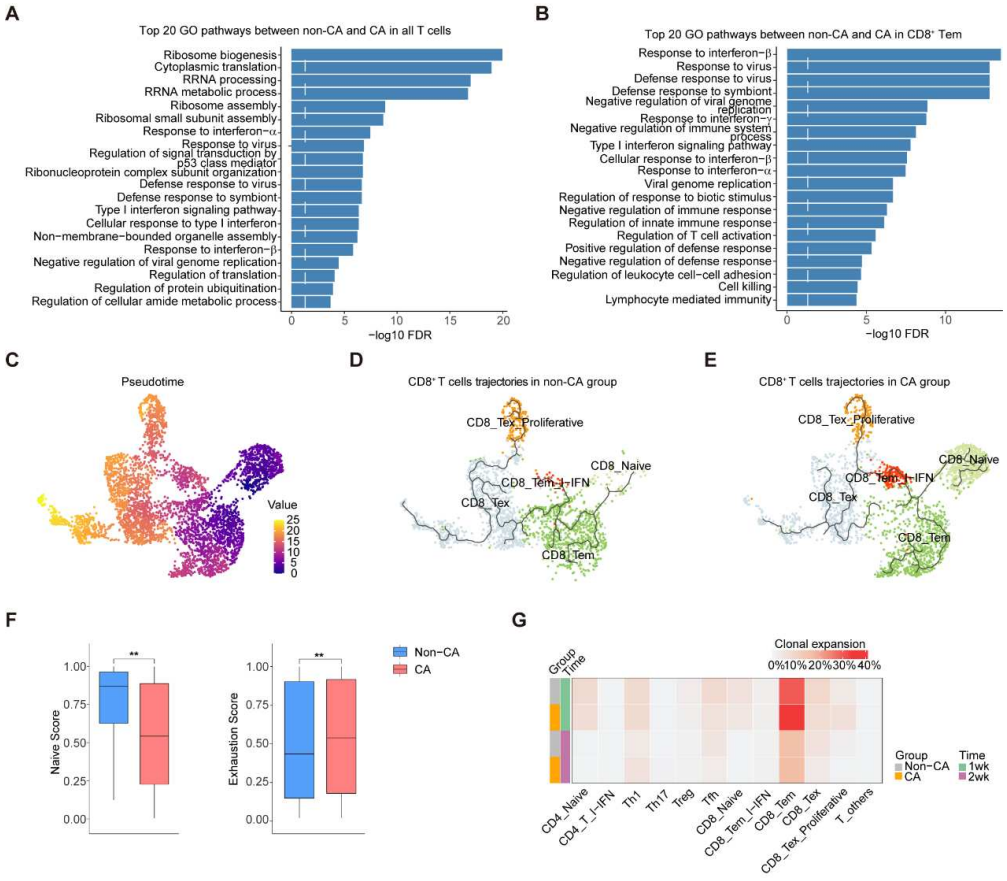

Supplementary Figure S5. Expansion of T cells exhibiting upregulated responses to type I IFN pathway and exhaustion features post-cryoablation.

(A and B) GO pathway enrichment analysis of all T cells and CD8+ effector memory T cells based on the DEGs between the non-CA and CA groups.

(C-E) The pseudotime developmental trajectory performed on CD8+ T cells. The graphs represent pseudotime values (C), pseudotime trajectory in the non-CA (D) and CA (E) groups.

(F) Box plot indicating naïve and exhaustion scores of CD8+ T cells at 1 week after cryoablation.

(G) Heatmap showing clonal expansion in T cell clusters across groups at 1 week and 2 weeks after cryoablation.

The statistical significance of differences between groups was determined by the nonparametric

Wilcoxon rank sum test with Bonferroni correction. **, P < 0.01. CA, cryoablation; non-CA, non-cryoablation.

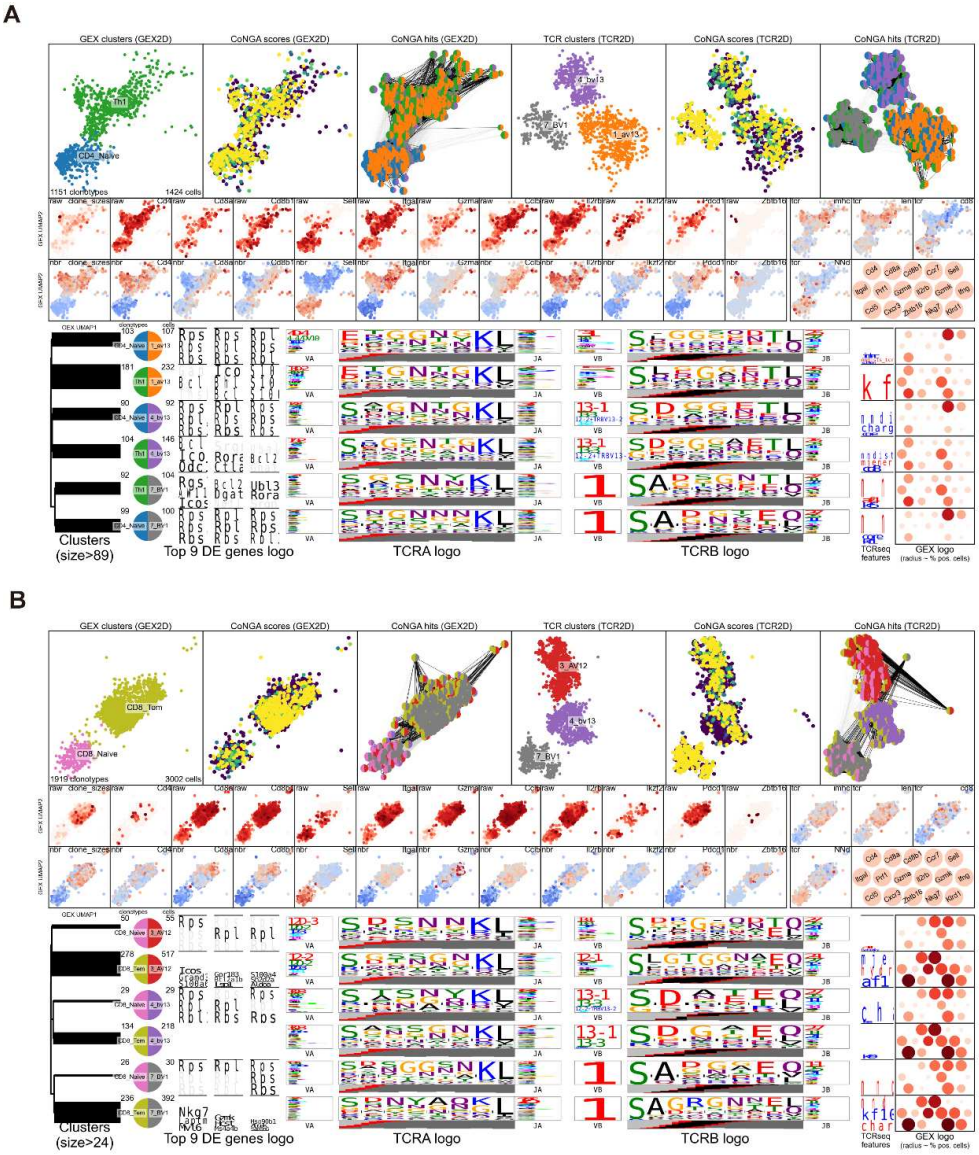

Supplementary Figure S6. Expansion of initially activated naïve T cells induced by cryoablation.

(A and B) CoNGA analysis of naïve CD4+ (A) and CD8+ (B) T cells.

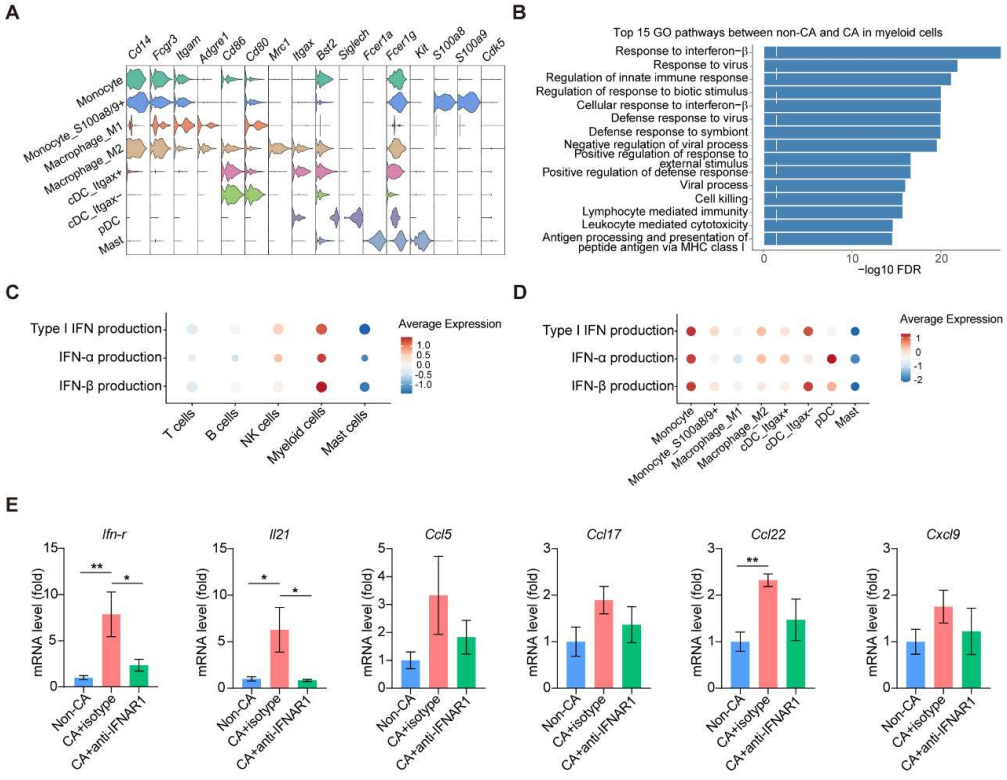

Supplementary Figure S7. Upregulation of responses to type I IFN in myeloid cells after cryoablation and changes of intra-tumoral cytokines and chemokines upon IFNAR1 blockade.

(A) Single-cell transcription level of representative genes illustrated in the UMAP plot of myeloid cells.

(B) GO pathway enrichment analysis of myeloid cells based on the DEGs between the non-CA and CA groups.

(C and D) Type I IFN production analysis in different cell types (C) and subpopulations of myeloid cells (D).

(E) mRNA levels of intra-tumoral cytokines and chemokines after the treatment of cryoablation combined with an anti-IFNAR1 blocking antibody or an isotype control monoclonal antibody (n =

5 per group).

The statistical significance of differences among multiple groups was determined by one-way ANOVA. *, $P < 0.05$; **, $P < 0.01$. CA, cryoablation; non-CA, non-cryoablation.